$\overline{\text{P}}$anda-MVD - note 007

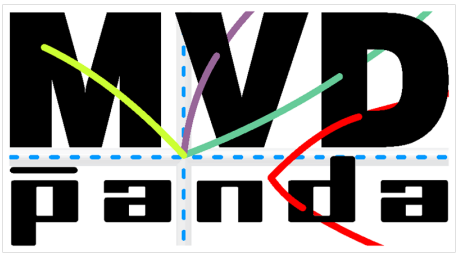

Rate Study in the Pixel part of the MVD

L. Zotti [1,2]
D. Calvo [2] , R. Kliemt [3]

[1] Turin University
[2] INFN Turin
Via P. Giuria 1, 10125, Turin, Italy
Email: zotti@to.infn.it
[3] Rheinische Friedrich-Wilhelms-Universität Bonn, Helmholtz-Institut für Strahlen- und Kernphysik
Nussallee 14-16, D-53115, Bonn, Germany

24/5/2011

Abstract

The particle rate information is of fundamental importance in the design of the detector. Indeed the particle rate determines not only the main features of the basic operation parameters of the readout electronics but also the cables design and the detector dead time. The aim of this work is the study of the particle rate with a particular attention to the pixel part of the MVD. The $\overline{\mathsf{p}} - \mathsf{p}$ and different $\overline{\mathsf{p}} - \mathsf{Nuclei}$ annihilations have been studied for different antiproton momenta, in order to estimate the rate that can be achieved in the $\overline{\mathsf{P}}\mathsf{ANDA}$ environment, no digitalization and no time information of the pellet targets is present.

1 Introduction

To evaluate the particle fluence on the pixel part of the $\overline{\mathsf{P}}$ANDA MVD, coming from the $\overline{\mathsf{p}}\mathsf{p}$ and $\overline{\mathsf{p}}\mathsf{N}$ annihilations, a series of simulations has been performed using the **Pandaroot** software [1].
In order to obtain the particle fluence in the pixel part of MVD we used:

- event generators;
- pixel detector geometry;
- GEANT4 as transport model [1];

In order to perform the simulations some dedicated macros have been written, which include:

- the geometry file of the detector and of the beam pipe with the relative materials composition and the magnetic field map;
- the background file produced by the event generators.

1.1 Event generators

For the simulation of the annihilation background the Dual Parton Model (DPM) based generator was used for the $\overline{\mathsf{p}} - \mathsf{p}$ annihilation and the Ultrarelativistic Quantum Molecular Dynamic Model (UrQMD) was used for $\overline{\mathsf{p}} - \mathsf{N}$ interaction.

1.1.1 The Dual Parton Model

The DPM is based on the application of the Regge theory [3]. The DPM generator allows to generate background events to the main channels, evaluate detector occupancies and particle rates [4], [5]. It is developed and maintained inside the $\overline{\mathsf{P}}$ANDA collaboration. During the DPM initialization it is possible to switch on and off the elastic and inelastic electromagnetic processes.

1.1.2 The Ultrarelativistic Quantum Molecular Dynamic Model

The UrQMD is a microscopic model based on a phase space description of a nuclear reaction [6]. It describes the phenomenology of hadronic interactions at low and intermediate energy ($\sqrt{s} < 5$ GeV) in terms of interactions between known hadrons and their resonances. At high energies the excitation of the colour strings and their subsequent fragmentation into hadrons are also taken into account.

[1] The physics list `QGSP_Bert_EMV` has been used for the physical processes which is the one suggested for simulation of the $\overline{\mathsf{P}}$ANDA events [2]. It produces particles in good agreement to experimental data.

1.2 Pixel detector geometry

To study the particle fluence in the pixel part we need the complete implementation of the geometry in a root-file. The geometry implementation takes advantage of the tools developed to convert the technical drawings created by Computer Aided Design (CAD) programs directly into root-file, that is used in the simulation.
The description of the pixel part, made of disks and barrel, is described in two different files:

- disk complete geometry: `Pixel-Fwd_Simplified_E.root`. It comprises only the disk part, and it is composed of sensors, carbon foam, electronic components and cooling pipes. It's a realistic geometry implementation, that is needed in order to know the fluence that we can expect.
- barrel complete geometry: `Pv-3_0-Pixel-HShell.root`. It comprises the barrel part, and it is composed, as the previous one, of all the components that will form the real detector.

In the following we list the number conventions, that will be used in the next sections for the analysis discussion.

1.2.1 Number Convention

For the barrel part, we define barrel 1 as the inner one, and barrel 2 to be the outer one. Besides, we assign increasing numbers to each stave, looking at the barrel along the antiproton direction in a clockwise order starting from the top, as shown in Fig.1. For the disk part we assign number 5 to the first disk in the forward direction starting from the interaction point, see Fig. 2.

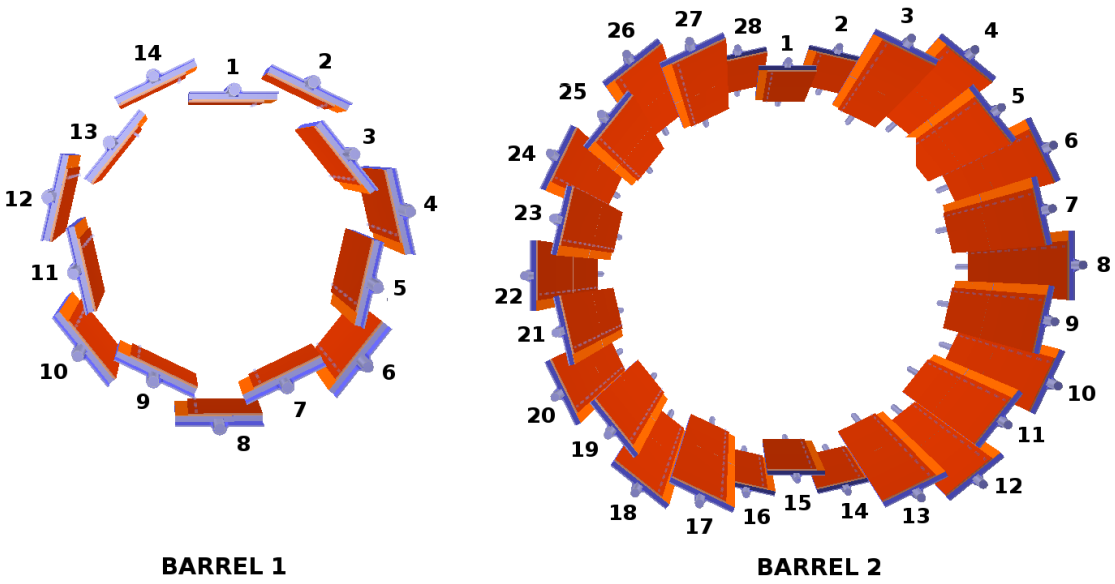

Figure 1: Convention numbers of the barrel part: on the left the inner barrel and on the right the outer one.

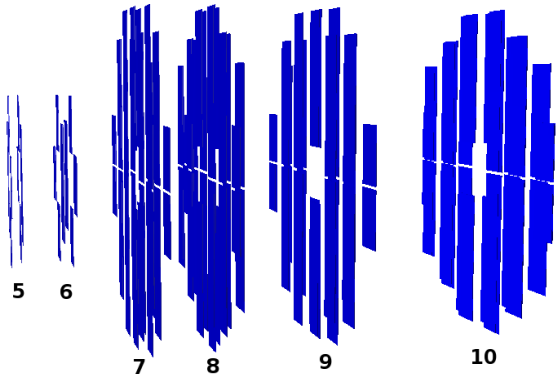

Figure 2: Convention numbers for the disk part.

2 $\overline{\mathsf{p}} - \mathsf{p}$ annihilations

As mentioned before the DPM model has been used to study the $\overline{\mathsf{p}} - \mathsf{p}$ annihilations. A preliminary study has been done using the `Mvd-v2.0_Sensors.root` geometry file, and exploring a large momentum range in order to be sure to include the elastic peak present in the $\overline{\mathsf{p}} - \mathsf{p}$ total cross section. One million of events have been simulated at different $\overline{\mathsf{p}}$ momenta, in particular in the range from 15 GeV/c down to 4 GeV/c. As shown in Fig. 3, the elastic component dominates the cross section for $\overline{\mathsf{p}}$ momenta below 10 GeV/c. From the DPM simulation, we found two elastic peaks,

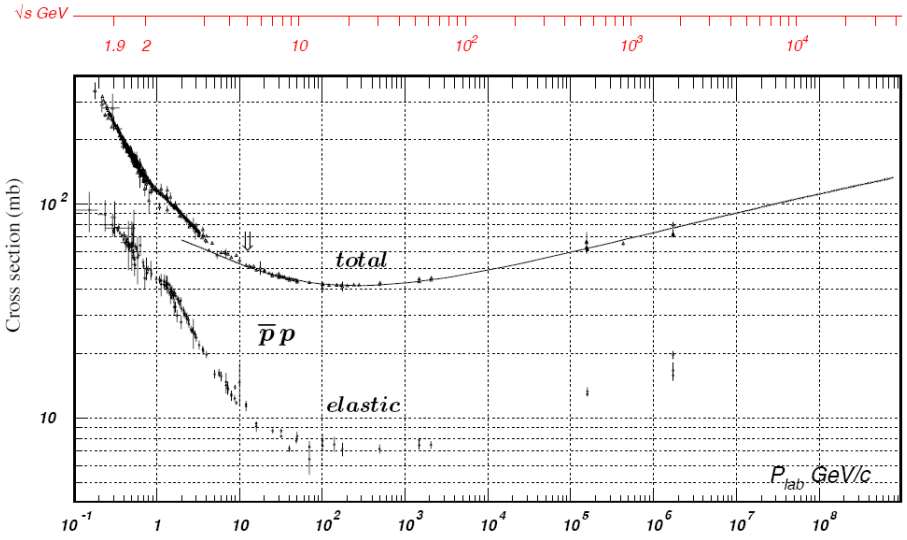

Figure 3: The $\overline{\mathsf{p}} - \mathsf{p}$ cross section, [7].

one of low energetic particles around $\theta = 90°$ (where θ is the angle with respect to the beam) and the other of high energetic particles at very small polar angles, as shown in Fig.4. In particular it is visible that most of the particles are going in the disk part of the MVD, i.e. with $\theta < 40°$. The maximum counts on the disk and

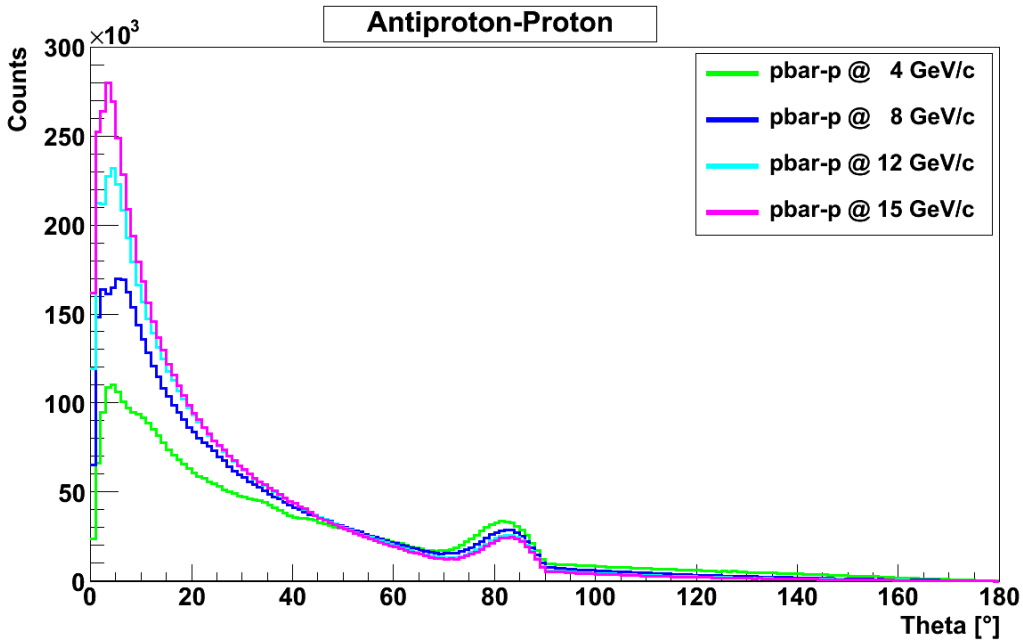

Figure 4: The particle theta distribution for $\overline{\mathrm{p}} - \mathrm{p}$ annihilations at different momenta (10^6 simulated events).

on the barrel part are listed in Tab. 2, for 10^6 simulated events. We find that the maximum count corresponds to the $\overline{\mathrm{p}}$ momentum of 15 GeV/c, and it is also evident that the maximum fluence will be on the disk part.

Momentum [GeV/c]	Disk Counts	Barrel 1 Counts	Barrel 2 Counts
4	4.8 M	3.9 k	7.5 k
8	6.5 M	3.0 k	6.1 k
11	7.1 M	2.6 k	5.6 k
12	7.3 M	2.5 k	5.5 k
13	7.4 M	2.5 k	5.8 k
14	7.5 M	2.4 k	5.3 k
15	7.8 M	2.4 k	5.3 k

Table 1: Particle counts on the different layer for different $\overline{\mathrm{p}}$ momenta (10^6 simulated events).

Using the `Pixel-Fwd_Simplified_E.root` geometry file, $8.5 \cdot 10^6$ $\overline{\mathrm{p}} - \mathrm{p}$ interactions at 15 GeV/c have been simulated, and we evaluate the number of hits on each disk. We calculate the flux for the foreseen annihilation rate of $2 \cdot 10^7$ s^{-1}. This flux will be indicated below as the "extrapolated" flux. The counts of each disk are listed in Tab.2.

The distribution of the hits is not uniform on the disk, as shown in Fig.5. The density of hits is high in the circular region around the beam pipe and decreases with increasing radius. The lepton flux is almost homogeneous, as shown in Fig.6,

Disk	Hadrons	Hadron Flux $[cm^{-2}\ s^{-1}]$	Leptons	Lepton Flux $[cm^{-2}\ s^{-1}]$
5	$5.22 \cdot 10^6$	$5.33 \cdot 10^5$	$3.10 \cdot 10^5$	$31.7 \cdot 10^3$
6	$7.41 \cdot 10^6$	$7.58 \cdot 10^5$	$5.93 \cdot 10^5$	$60.6 \cdot 10^3$
7	$13.3 \cdot 10^6$	$2.11 \cdot 10^5$	$1.52 \cdot 10^6$	$24.1 \cdot 10^3$
8	$13.9 \cdot 10^6$	$2.21 \cdot 10^5$	$2.04 \cdot 10^6$	$32.5 \cdot 10^3$
9	$13.7 \cdot 10^6$	$2.17 \cdot 10^5$	$2.35 \cdot 10^6$	$37.3 \cdot 10^3$
10	$9.84 \cdot 10^6$	$1.56 \cdot 10^5$	$2.13 \cdot 10^6$	$33.8 \cdot 10^3$

Table 2: Numbers of hits for hadrons and leptons on the different MVD disks for $8.5 \cdot 10^6$ events simulated and fluxes evaluated taking into account the $\overline{\mathsf{P}}$ANDA annihilation rate.

considering that 88% of the leptons are not primary particles.

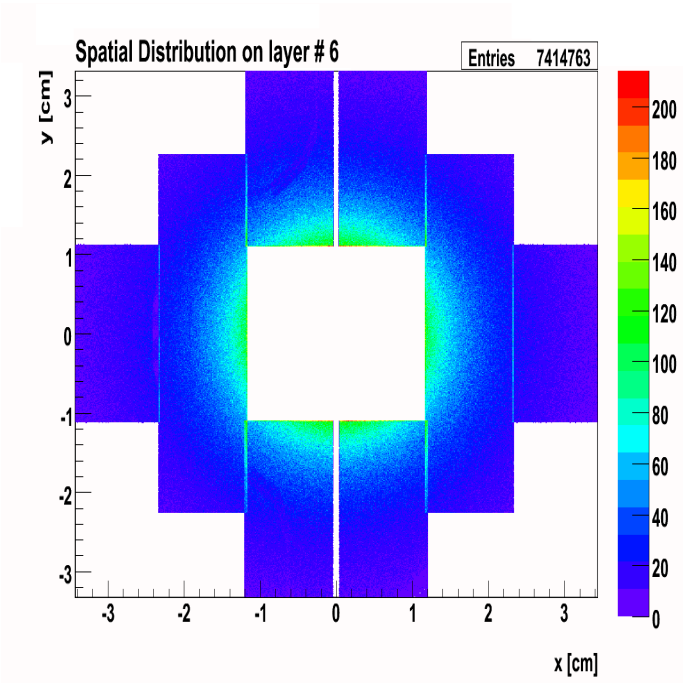

Figure 5: Hadron hits distribution on disk number 6.

In conclusion the expected extrapolated maximum hadron flux is $\sim 6 \cdot 10^6\ cm^{-2}\ s^{-1}$, while the maximum expected lepton flux is $\sim 4 \cdot 10^4\ cm^{-2}\ s^{-1}$, without digitalization and time information.

3 $\overline{\mathsf{p}}$ – Nucleus annihilations

For the study of $\overline{\mathsf{p}}$ – Nucleus annihilation we used the UrQMD model as event generator. Three different annihilations: $\overline{\mathsf{p}} - \mathsf{N}$, $\overline{\mathsf{p}} - \mathsf{Ar}$ and $\overline{\mathsf{p}} - \mathsf{Au}$ have been studied. As shown in Fig.7, the angular distribution of the emitted particles is more homogeneous along the theta angles, and in the case of $\overline{\mathsf{p}} - \mathsf{Au}$ annihilations there is a peak around 90°, so as far as the hit distribution is concerned also the barrels have to be taken into account.

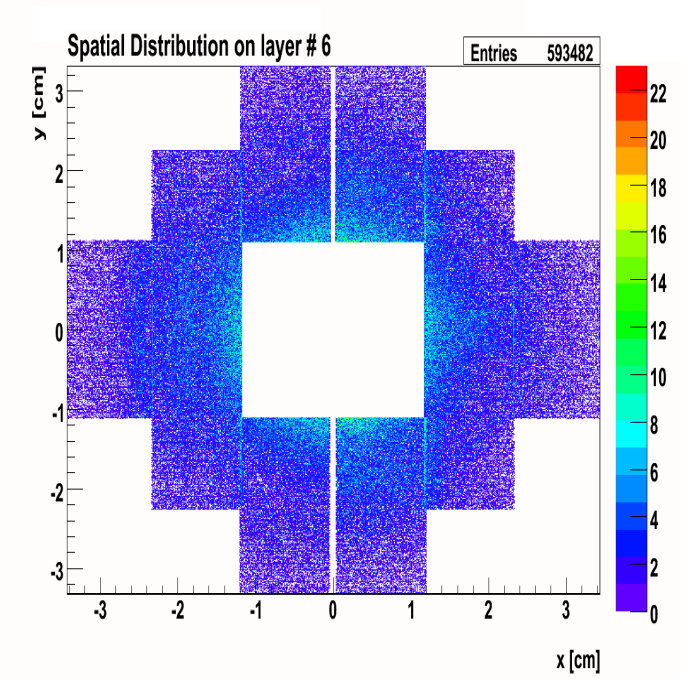

Figure 6: Lepton hits distribution on disk 6.

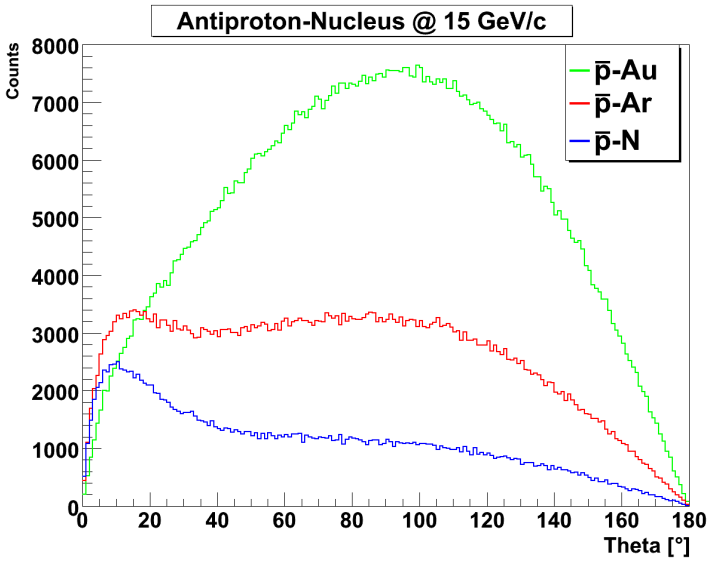

Figure 7: Theta distribution for different $\bar{p} - N$ annihilations

Using the `Pixel-Fwd_Simplified_E.root` and `Pv-3.0-Pixel-HShell.root` geometry files, we have simulated $2.5 \cdot 10^6$ events for each of these reactions. The maximum hadron and lepton fluxes, see Tab.4, Tab.5 and Tab.6, have been obtained multiplying a scaling factor that takes into account the maximum average luminosity achievable for the considered nuclei, see Tab. 3.

Nucleus	Maximum Average Luminosity $[cm^{-1}\ s^{-1}]$
$\overline{\mathsf{p}} - \mathsf{N}$	$9.0 \cdot 10^{31}$
$\overline{\mathsf{p}} - \mathsf{Ar}$	$2.4 \cdot 10^{31}$
$\overline{\mathsf{p}} - \mathsf{Au}$	$2.2 \cdot 10^{30}$

Table 3: Expected maximum average luminosity for beam momentum of 15 GeV/c [6].

Nucleus	Hadron Flux $[cm^2\ s^{-1}]$	Disk N.	Lepton Flux $[cm^2\ s^{-1}]$	Disk N.
$\overline{\mathsf{p}} - \mathsf{N}$	$5.80 \cdot 10^5$	6	$3.75 \cdot 10^4$	6
$\overline{\mathsf{p}} - \mathsf{Ar}$	$3.20 \cdot 10^5$	5	$1.50 \cdot 10^4$	6
$\overline{\mathsf{p}} - \mathsf{Au}$	$9.34 \cdot 10^4$	5	$1.25 \cdot 10^3$	5

Table 4: Maximum hadron and lepton extrapolated flux on the disk region.

Nucleus	Hadron Flux $[cm^2\ s^{-1}]$	Lepton Flux $[cm^2\ s^{-1}]$
$\overline{\mathsf{p}} - \mathsf{N}$	$3.12 \cdot 10^5$	$6.37 \cdot 10^3$
$\overline{\mathsf{p}} - \mathsf{Ar}$	$2.52 \cdot 10^5$	$3.60 \cdot 10^3$
$\overline{\mathsf{p}} - \mathsf{Au}$	$1.03 \cdot 10^5$	$5.77 \cdot 10^2$

Table 5: Maximum hadron and lepton extrapolated flux on the first barrel.

Nucleus	Hadron Flux $[cm^2\ s^{-1}]$	Lepton Flux $[cm^2\ s^{-1}]$
$\overline{\mathsf{p}} - \mathsf{N}$	$7.25 \cdot 10^4$	$3.60 \cdot 10^4$
$\overline{\mathsf{p}} - \mathsf{Ar}$	$5.77 \cdot 10^4$	$2.06 \cdot 10^4$
$\overline{\mathsf{p}} - \mathsf{Au}$	$2.26 \cdot 10^4$	$3.94 \cdot 10^3$

Table 6: Maximum hadron and lepton extrapolated flux on the second barrel.

The maximum particle rate takes into account both the hadron and lepton fluxes and it is listed in Tab. 7. In the case of $\overline{\mathsf{p}} - \mathsf{N}$ and $\overline{\mathsf{p}} - \mathsf{Ar}$, the maximum rate is on the disk part, and as in the case of $\overline{\mathsf{p}} - \mathsf{p}$ the hit distribution is not homogeneous, so we refer to the maximum rate as the one in the circular region around the beam pipe.
In the case of $\overline{\mathsf{p}} - \mathsf{Au}$, the maximum hadron rates will be in the first barrel part. The distribution of the particle hits, as shown in Fig.8, is non-homogeneous, since there is a region of the stave near z=0 that is hit by the most hadrons. Focusing the attention on the zone of highest hit rate (-1 cm $<$ z $<$ 1 cm) we obtain an extrapolated flux of

Nucleus	Average Rate $[cm^2\ s^{-1}]$	Maximum Rate $[cm^2\ s^{-1}]$	Region
$\overline{\mathrm{p}} - \mathrm{N}$	$6.20 \cdot 10^5$	$1.23 \cdot 10^6$	Disk
$\overline{\mathrm{p}} - \mathrm{Ar}$	$3.30 \cdot 10^5$	$6.80 \cdot 10^5$	Disk
$\overline{\mathrm{p}} - \mathrm{Au}$	$1.03 \cdot 10^4$	$1.60 \cdot 10^5$	Barrel

Table 7: Average and maximum rates for different $\overline{\mathrm{p}}$-Nuclei evaluated taking into account the corresponding maximum luminosity (Simulated events: $2.5 \cdot 10^6$).

$\sim 16 \cdot 10^4$ hits $cm^{-2}\ s^{-1}$. The maximum lepton flux is registered on the second barrel, where we find $\sim 4 \cdot 10^3\ cm^{-2}\ s^{-1}$. As shown in Fig.9, the lepton hit distribution is almost homogeneous.

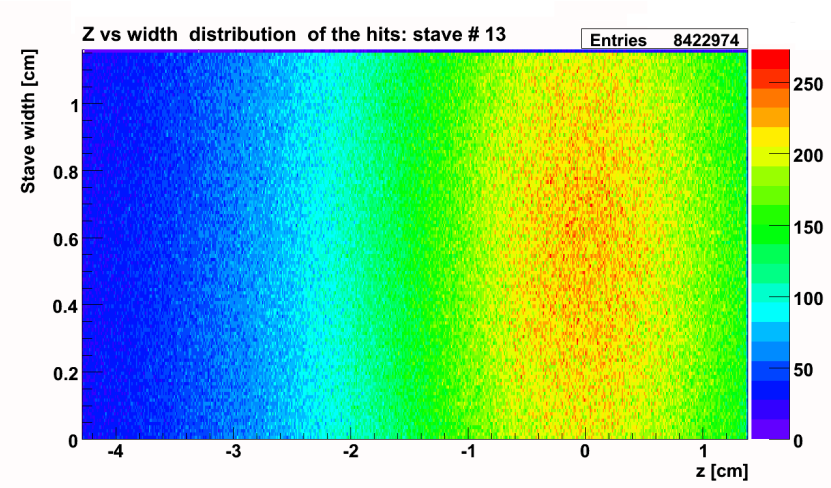

Figure 8: Distribution of the hadron hits on the stave number 13, the stave width is plotted as a function of the z coordinate.

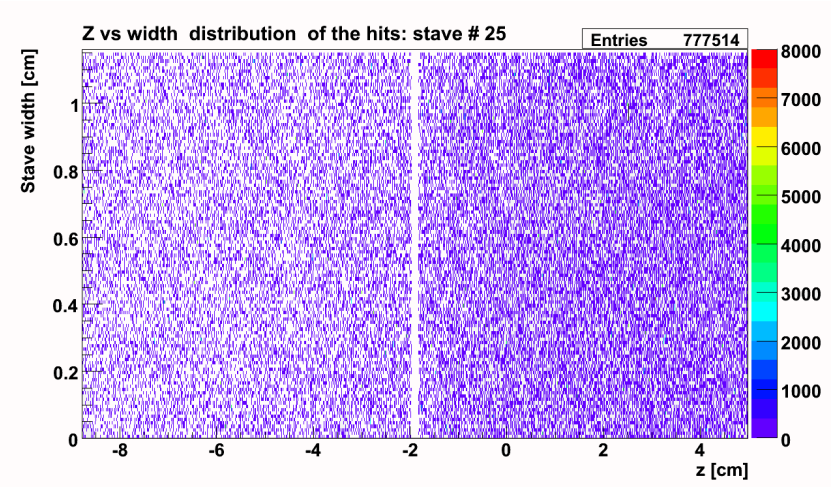

Figure 9: Lepton distribution on the stave number 25 of barrel 2, the stave width is plotted vs the z coordinate.

4 Comparison with previous rate study

The main differences with the previous rate study [8] are:

- the MVD geometry files used as input in the simulation are different: in [8] the `MVD-1.0 Pv-1.0 Sv-1.0.root` was used. It differs from the geometry used in this work, in the pixel sensors dimensions and in the position of the disks.
- In [8] the $\overline{\mathsf{p}} - \mathsf{Au}$ annihilation study was performed within the old Pandaroot framework.
- In this work no digitization is present, and only the pixels are present.
- The statistics is quite big respect to the one present in [8] where at maximum 10^6 events for each annihilations have been simulated.
- No safety factor has been introduced here.

Nevertheless some comparison can be done taking into account the intrisic features of the two works.
As show in Tab.8 and Tab.9 the particle rate in the two annihilations case are of the same order of magnitude. In particular we scaled the maximum count rate of [8] dividing for the safety factor (4), the readout area and the pixel cluster size in the case of a thickness of 200 μm (that has an average value of 2.5 pixels).

Study	Simulated Events	Particle Rate $[cm^{-2}s^{-1}]$
Previous	$4 \cdot 10^4$	$3.64 \cdot 10^6$
This	$8.5 \cdot 10^6$	$6 \cdot 10^6$

Table 8: Comparison with previous rate study for the $\overline{\mathsf{p}} - \mathsf{p}$ annihilations 15 GeV/c, the particle rate is normalized to $2 \cdot 10^7$ annihilations/s.

Study	Simulated Events	Particle Rate $[cm^{-2}s^{-1}]$
Previous	10^6	$1.11 \cdot 10^5$
This	$2.5 \cdot 10^6$	$1.6 \cdot 10^5$

Table 9: Comparison with previous rate study for the $\overline{\mathsf{p}} - \mathsf{Au}$ annihilations 15 GeV/c, the particle rate is normalized to $2 \cdot 10^5$ annihilations/s.

5 Conclusion

The estimate of the particle rate addresses the important question of the maximum average luminosity that the detector can manage. The important aspect in the rate estimation is the initial interaction rate, that changes depending on the target; a precise knowledge of the beam conditions and of the available target is necessary. Indeed the rates could be different in the case of the jet-target. Moreover a time dependent annihilation rate should be implemented, in order to have not only an average information but also to take into account the peak rates due to possible overlap of the pellets-target.

References

[1] http://panda-wiki.gsi.de/cgi-bin/view/Computing/PandaRoot

[2] http://geant4.web.cern.ch/geant4/support/index.shtml

[3] $\overline{\mathsf{P}}$ANDA Collaboration, Technical Progress Report, http://www-panda.gsi.de/auto/_home.htm

[4] Uzhinsky et al., Cross Sections of Various Processes in Pbar P-Interactions, arXiv:hep-ph/0212369 (2002)

[5] A. Galoyan et al., Parametrization of the $\overline{\mathsf{P}}\mathsf{P}$ Elastic Scattering Differential Cross Section Between 2 GeV/c $\leq \mathsf{P}_{\mathsf{lab}} \leq$ 16 GeV/c,

[6] $\overline{\mathsf{P}}$ANDA Collaboration, Physics Performance Report for $\overline{\mathsf{P}}$ANDA, arXiv:0903.3905v1 (2009)

[7] http://pdg.lbl.gov/2010/reviews/rpp2010-rev-cross-section-plots.pdf

[8] M. Mertens, Th. Würschig, R. Jäkel, Count rate studies for the Micro-Vertex-Detector, Panda-MVD-note 4,